Implementation of a Mesomechanical Material Model for IAD Fabrics within LS-DYNA®

AE 8900 MS Special Problems Report
Space Systems Design Lab (SSDL)
Guggenheim School of Aerospace Engineering
Georgia Institute of Technology
Atlanta, GA

Author:
Jeremy Hill

Advisor:
Dr. Robert D. Braun

December 14, 2012

Implementation of a Mesomechanical Material Model for IAD Fabrics within LS-DYNA®

Jeremy L. Hill[1] and Robert D. Braun[2]
Georgia Institute of Technology, Atlanta, GA, 30332-0150

The implementation and evaluation of a high fidelity material model for dry fabrics is the main objective of this paper. Inflatable Aerodynamic Decelerators (IADs) and other air-inflated structures quite often utilize woven fabrics due to their lightweight and high loading carrying capabilities. Design optimization of these inflated structures relies on a detailed understanding of the woven fabric mechanics. Woven fabrics are composite orthotropic materials that respond differently under load from traditional solid mechanics. While low-fidelity fabric materials usually assume a continuous medium, a higher fidelity model needs to account for the reorientation of yarns and weave geometry. An existing mesomechanical material model within the LS-DYNA® commercial non-linear finite element software package is utilized. In this paper, experimental stress-strain data for Kevlar 129 samples are validated against numerical simulations of models with matching geometry and loading conditions.

Nomenclature

E	=	Elastic Modulus
G	=	Shear Modulus
ρ	=	Mass Density
v	=	Poisson's Ratio
β	=	Undulation Angle
θ	=	Braid Angle
θ_{lock}	=	Locking Angle of Yarns
$\Delta\theta$	=	Angle Tolerance for Locking
μ	=	Shear Resistance Discount Factor
q	=	Yarn Unit Direction Vector
F	=	Deformation Gradient

Subscripts

1	=	Yarn Longitudinal Direction
2	=	Yarn Lateral Direction
12	=	Plane Defined by 1, 2 axes
23	=	Plane Defined by 2, 3 axes
f	=	Fill
w	=	Warp

Acronyms

IAD	=	Inflatable Aerodynamic Decelerator
EDL	=	Entry, Descent, and Landing
IRVE	=	Inflatable ReEntry Vehicle Experiment

[1] Graduate Research Assistant, Daniel Guggenheim School of Aerospace Engineering, AIAA Student Member.
[2] Professor, Daniel Guggenheim School of Aerospace Engineering, AIAA Fellow.

I. Introduction

PLANS for future Mars missions involve placing larger and heavier payloads on the surface. Currently, supersonic parachutes place difficult constraints on the available payload mass. In the late 1960's and early 1970's NASA began initiating technology programs aimed at maturing Inflatable Aerodynamic Decelerators (IADs). Compared to supersonic parachutes, Supersonic and Hypersonic IADs represent a decelerator option that provides a large drag area capable of operating at higher Mach numbers and dynamic pressures. This characteristic translates to being able to deploy earlier in the Entry Decent Landing (EDL) timeline and opens the design space to higher elevation landing sites[1]. After a couple decades of little to no acknowledgement, IADs saw resurgence in interest from the EDL community in the early 2000's[2]. Technology investments in the last decade have significantly progressed three IAD configurations: the attached isotensoid, tension cone, and stacked toroid[3,4,5]. An example illustration of the stacked toroid configuration is provided in Figure 1.

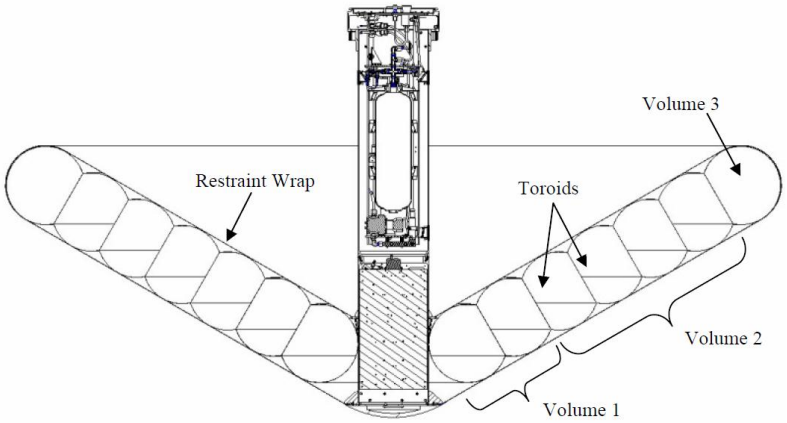

Figure 1: IRVE Stacked Toroid[5]

In a historical look at IAD development, Smith et al mentions aerodynamics, static and dynamic stability, aerothermodynamic loading, structural analysis and testing, inflation, and materials as essential areas for IAD maturation[6]. Both computational and experimental research advancements are still needed before IADs can be employed in future missions. Subscale or ground based experimental testing is difficult and expensive to carry out. It will likely be that computational analysis will fill the gap and extend the analysis beyond experimental testing limitations. The Fluid Structure Interaction (FSI) associated with IADs is of particular importance because it is an analysis that addresses the coupling aerodynamic and structural behavior. Tanner's work with FSI dealt with, in a broad sense, the framework necessary to couple fluid and structural solvers[7]. His framework has the advantage of being adaptable to virtually any suite of CFD and FEM solvers. Having said that, this architecture is limited by the numerical tools it employs. In Tanner's FSI analysis, it was shown that the finite element model was overly stiff when compared to deflections seen in the wind tunnel[7]. Because FEA will only be as accurate as the inputs, two areas in need of advancement are the modeling of IAD materials, as well as, the determination of the mechanical properties that serve as inputs to the models. IADs and other air-inflated structures quite often utilize woven fabrics due to their lightweight and high loading carrying capabilities. Design optimization of these inflated structures relies on a detailed understanding of the woven fabric mechanics.

As a secondary motivation, the influence of material properties on IAD mass was explored. Samareh presents a technique for estimating the mass of IADs using a set of dimensionless parameters relating to the inflation gas mass, inflation pressure, and flexible material mass[8]. The methodology is applicable for trailing IADs, tension cones, and stacked toroids. For this study, the stacked toroid with coated fabric (Case 4) was chosen for consideration. The equations derived in the literature were implemented in MATLAB. It was observed that material properties were included in several equations, but the largest contributor to mass was the estimate for minimum inflation pressure. Samareh uses an approach for estimating the minimum inflation based on the principle of virtual work. Fundamentally, the external work from the aerodynamic forces must be balanced by the internal work of the gas. The resulting equation is a function of the drag load on the decelerator and geometry. From this, one could look at

how changing minimum inflation pressure affects IAD mass. The analysis showed that for case 4, minimum inflation pressure was close to 5 psi. The next step was to obtain a realistic estimate for how material properties affect minimum inflation pressure in stacked toroids. To simplify this effort, the buckling load of single toroid was examined. Kyser presents a study that looks at some basic questions associated with the use of inflated toroids within IADs[9]. The paper examines the load carrying capabilities and failure modes of a toroid during and after deployment. Kyser provides relations for the critical buckling load of a slender thin-walled pressurized toroidal shell subjected to a uniform radial compressive load. Both the equations for in and out of plane buckling are functions of the elastic and shear modulus of the wall. While these equations are for a single toroid and assume an isotropic material, the general trends can be utilized. Now that the material properties of the fabric can be related to the minimum inflation pressure to resist buckling, perturbations to the elastic and shear modulus were applied to observe how critical buckling load varies. Examples of uncertainty in moduli were taken from Hutchings, in which uniaxial and estimated biaxial moduli are presented[10]. The estimated biaxial modulus is almost 2/3 of the uniaxial modulus. With this, all the necessary information to complete this secondary study was obtained. On the left side of Figure 2, the variation of critical buckling load with scaled modulus values is shown. In addition, the impact of changes in the minimum inflation pressure on inflatable mass, for this example, is shown on the right in Figure 2.

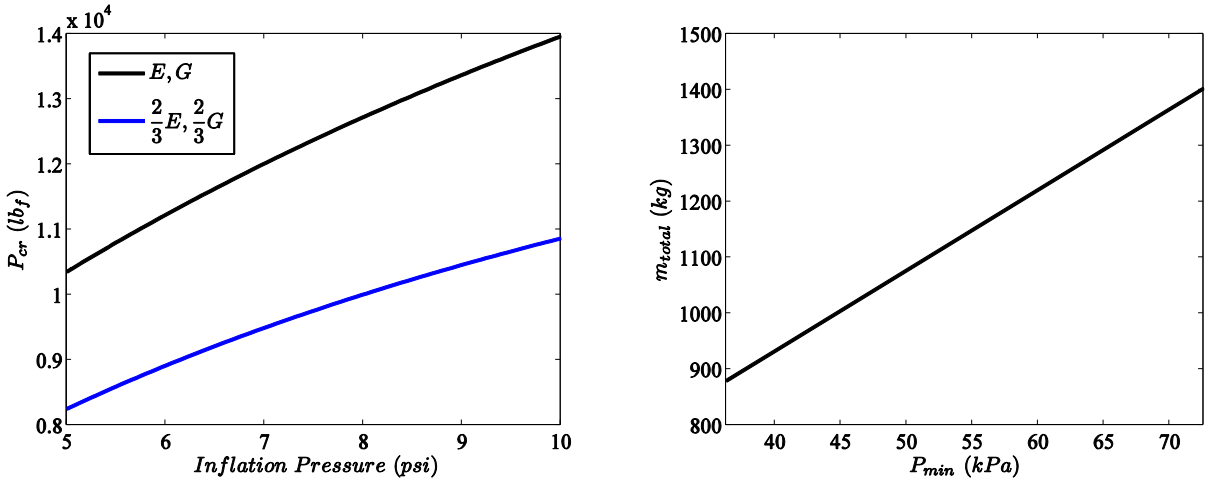

Figure 2: Critical Buckling Load (Left) and Total Inflatable Mass (Right)

Keeping in mind that minimum inflation pressure for the stacked toroid was approximately 5 psi, the inflation pressure was varied from 5 to 10 psi. It is seen in the above plot on the left, that in order to maintain the same buckling load, the reduced moduli toroid must increase inflation pressure from 5 to 8.7 psi. So, the toroid would need to be inflated to nearly double the internal pressure to resist the same uniform radial load. Applying a factor of 2 increase in minimum inflation pressure to the mass estimate, it can be seen on the right of Figure 2, that the mass of the inflatable increases by approximately 59%. This further emphasizes the point that a detailed understanding of the woven fabric mechanics is necessary for the design of inflated structures.

II. Textile Modeling

A great deal of work has been done to better determine the mechanical properties of fabrics experimentally. Basset et al. reviews several experimental methods for determining fabric elastic and shear moduli. Biaxial tension, Shear, and Bias extension testers measure one of the mechanical properties while keeping the others constant or zero. Combined testers like the inflated cylinder test utilize hydrostatic pressure, axial force, and torsion to simultaneously vary the state of stress[11]. Hutchings utilized several of these experimental test methods to obtain experimental data for candidate IAD orthotropic materials[10]. The material data that was obtained from this testing was utilized in the FSI work of Tanner. Similar test methods were used in a combined effort between NASA and ILC Dover to carry out an experimental program to better characterize the stiffness of coated woven fabrics[12]. The results of which are intended to support a ground test campaign for inflatable decelerators. Tanner and Hutchings both acknowledge the benefit of a more detailed characterization of woven fabric material properties as the limitations of the experimental studies only provide an incomplete picture. In addition to the experimental work, a great deal of work has been done to better model the behavior of fabrics. Most models treat the fabric as a homogeneous material. To date, IAD

structural modeling has treated the fabric as a continuum. Even making the assumption of a continuous medium, the material has been modeled with isotropic and orthotropic material properties. In reality, a fabric is a complex structure of individual fibers that have been collected into yarns and interlaced together. More appropriate models exist that are dependent on variables such as individual fiber thickness, undulation angles, and fiber strengths, but determination of meso and micro mechanical properties can be difficult. Murman et al addresses several modeling techniques that can be used to capture some of the complex fabric responses[13]. Murman and Hutchings both allude to the use of advanced material models for IAD fabrics. However, they also note that detailed modeling of fabrics at the yarn or fiber level is computational intensive and not currently feasible for full-scale modeling.

As the purpose of this paper is to utilize a material model that accounts for the reorientation of the yarns and the fabric architecture, an overview of some fabric terminology is beneficial. Basically, fabrics are flexible materials that are constructed by interlacing yarns together. The yarns are composed of thousands of fibers or filaments that are combined together in some fashion (with or without twist) to form a textile fabric. A fiber is a strand of matter that is either organic or synthetic. It is the most fundamental element of a fabric. A filament is a single long fiber. Synthetic fibers are typically produced as a single filament. Textile fabrics represent a vast amount of unique constructions of materials ranging from individual fibers that are not woven to groups of fibers that are interlaced (weaved or braided) or interloped (knitted) together. Fabrics can be constructed using various methods and take on many patterns[14]. This paper focuses primarily on woven fabrics. A woven fabric is produced by interlacing two sets of yarns perpendicular to each other. The yarns running in the length direction of the fabric are called the warp yarns. Those running in the width direction of the fabric are called the weft or fill yarns. Fabrics can be constructed all from the same material or by organizing different materials to meet structural requirements. From this it can be seen that, for a given type of material, the physical properties and mechanical performance of the textile fabric are strongly dependent on the how it is structured. There are many ways of interlacing the warp and fill yarns into a fabric; the resulting layout is called the weave. When woven fabrics have considerable thickness due to multiple sets of yarns in the warp and fill directions, they are termed 3D fabrics. The detailed modeling of mechanical properties of woven fabrics has been the primary focus of some researchers for many decades; in areas ranging from the clothing industry to many engineering applications. Historically, models for woven fabrics have lagged behind other materials due to their complex nature[15]. Woven fabrics are composite orthotropic materials that respond differently from traditional solid mechanics. Terms like friction, crimp interchange, slip, and locking are used to describe the behavior of the fabrics under loading. Friction refers to the contact friction that exists between overlapping yarns. Crimp interchange is the shifting of undulation from the warp to the fill yarns or vice versa as a result from applied loading. These are important and are also affected by the type and manner of loading. Slip occurs as the yarns rotate due to shearing and locking occurs when the yarns jam together and can no longer rotate. The interactions that occur at the yarn and fiber level require a high level of detail at the expense of increased computational difficulty.

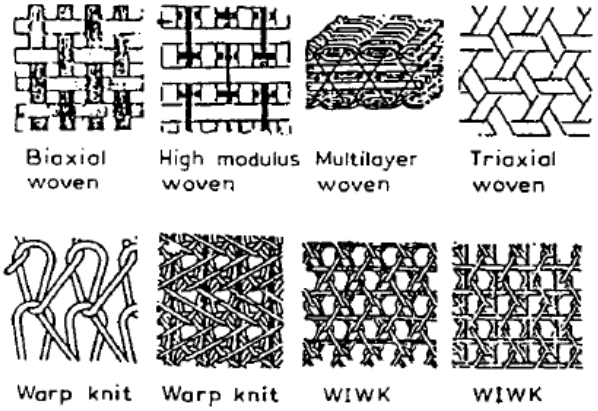

Figure 3: Examples of Woven, Braided, and Knitted Textile Patterns[14]

A woven fabric can be explored at three levels: Macroscopic, Mesoscopic, and Microscopic. Illustrations of the three levels of modeling are provided in Figure 4. The macroscopic level refers to the entire structure level, with dimensions on the order of meters. At this level, the fabric is seen as a continuum with orthotropic material properties and low shearing and bending stiffness. This is the level at which current IAD modeling efforts reside due to the ability to model large complex geometries. While there has been much work done in this area, there is no universally accepted model that accurately captures all aspects of the fabric's mechanical behavior. Some authors have proposed different macroscopic techniques for replicating the unique behavior of woven fabrics. Currently, most studies on inflated structures involve the testing of an inflated beam under various loading conditions and making observations about the structures response. Kabche et al experimentally tested inflated beams with applied tension and torsion loads[16]. In addition, the fabric moduli that were found experimentally were used in a finite element model to predict the response of the beam in bending. It was shown that the elastic and shear moduli of the

fabric varied as a function of inflation pressure, material properties of the fibers, and the structure of the weave. These are very useful observations, but require large amounts of testing and quantitative results are only applicable to the fabric under consideration. Cavallaro experimentally and analytically tested the bending response of an inflated beam. In addition, the micro and meso mechanical effects were studied through finite element modeling. It was observed that a model which included each warp and weft tow, as well as, their interactions was not possible computationally. A small unit cell was analyzed and the determined material properties were used in a global model of the inflated air beam. The results showed that the finite element model was stiffer than the experimental results. This was due to finite element model employing constant elastic and shear moduli, while the experimental material properties varied during loading[17].

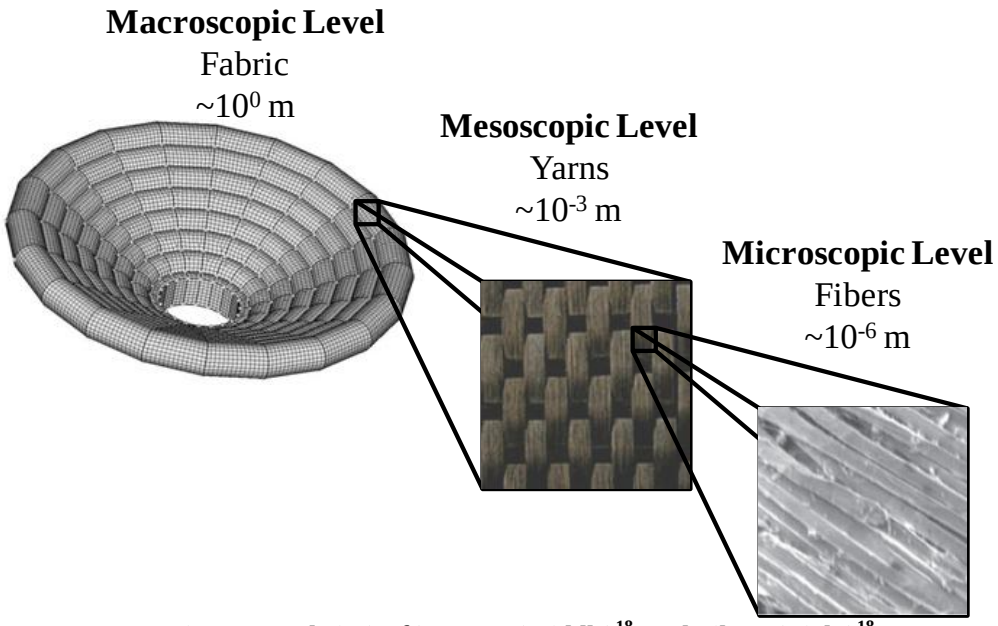

Figure 4: Fabric (Left), Yarns (Middle)[18], and Fibers (Right)[18]

At the mesoscopic level, the fabric is viewed as a series of interlacing tows called the warp and fill yarns and is usually on the order of several millimeters. This level of modeling usually considers the smallest repeating pattern that can properly represent the fabric under loading conditions. This area is usually termed the representative unit cell (RUC). Peng utilizes a novel approach for predicting the effective nonlinear elastic moduli of a textile fabric. A RUC was built and various numerical tests, like uniaxial tension testing and shear testing were carried out. Force vs. Displacement curves are obtained and the results are imposed on a four node shell element that can be applied to large scale model[19]. In most literature, each yarn is modeled as a continuum with its own constitutive law. In reality an IAD fabric can be composed of several thousands of yarns which are then composed of several thousands of continuous fibers that, at some extent, interact with each other. These interactions can be analyzed at the microscopic scale; with the working scale being on the order several micrometers. From a modeling standpoint, the fibers can be represented as beam elements that come into contact with their neighbors. This approach has been used to model small unit cells[17]. However, due to computational limitations, the numbers of fibers that can be modeled are limited and as a result so are the conclusions that can be drawn.

LS-DYNA® is the commercial non-linear finite element software package used extensively by the IAD community. Because of this, it is used for the work herein. Most structural analysis of IADs utilize LS-DYNA®'s standard fabric model (MAT_FABRIC). This planar orthotropic material model utilizes a 3 or 4 node shell element formulation. This macroscopic level model uses Hooke's law as the constitutive equation. The degree of homogenization utilized in this model makes it computationally desirable. However, it ignores many of the meso and microscopic interactions between yarns and fibers that can significantly influence the response of a fabric. A few of the literature sources interchange the terms meso and micro in their work, but are consistent in their approach of modeling at the yarn level. There are already existing material models within LS-DYNA® that model the mesomechanical behavior of fabric. Tabiei and Ivanov present such a material model that is later implemented in LS-DYNA®. The material

model (MAT_MICROMECHANICS_DRY_FABRIC) models the fabric on the yarn level. The model accounts for the reorientation of yarns and weave geometry[20]. It incorporates a homogenization technique; making it viable for large scale analyses. Prior IAD studies use the lack of published material data and unusual input parameters as reasons for not utilizing such material models.

III. Modeling Parameters

A. Candidate Material

In order to validate the material model, experimental data was sought that could be compared against the numerical solution. The goal was to simulate the same loading conditions used to obtain the experimental data. The stress vs. strain response from the simulation is then compared directly to the experimental data to observe whether or not the dual behavior of the fabric is represented. The dual behavior comes from the fact that initially the fabric is similar to a trellis mechanism; with large rotations of the yarns until some locking angle when then fabric begins to behave similar to a continuum. Because textile fabrics come in many forms, experimental data was sought that matched the assumptions of the material model. The model is derived for a plain weave fabric absent of any matrix or coating. Several literature sources were found that contained fabrics and their material properties that matched these assumptions. Difficulty arises when searching for yarn material properties and fabric architectures that go along with experimental fabric data. It is unlikely to find a data source that includes fabric test data, as well as, the required yarn data. Along with their development of the material model explored in this study, Tabiei and Ivanov also provide numerical results from a ballistic impact simulation. They provide the necessary inputs associated with a Kevlar 129 fabric. This made Kevlar 129 a desired material for this study. With the yarn elastic properties and fabric architecture obtain, the search was turned to the test data for validation purposes. The material testing done by Lin et al provided data necessary for comparison. The fabrics included in their experimental study were Nylon, Nomex, and Kevlar. These fabrics were selected because their relevancy to NASA ground test program for inflatable decelerator material technology. Both Kevlar 29 and 129 were included in the study. Kevlar 29 was used in the bladder of the IRVE-II flight test article, while Kevlar 129 was used in the structural spars. It was observed, however, that both of these materials were tested with a silicone coating. This could pose a problem as this material model is for a dry fabric. If the experimental data was to be used for validation purposes, it would need to be shown that the coating did not significantly affect the reorientation of the yarns. To do this, the two Kevlar materials were compared to each other. Figure 5 provides the axial stress vs. axial strain curves for both Kevlar 29 (200 Denier) and Kevlar 129 (840 Denier). The data corresponds to the 1st ramp up loading cycle in the warp direction. Ignoring that the 840 denier material was tested to higher stress, an interesting trend can be observed at the lower strain values. It has already been explained that in the early phases of loading, fabrics undergo crimp interchange and yarn reorientation that effectively results in a lower stiffness until locking occurs. The 200 denier material appears to transition quickly to having a linear elastic modulus, while the 840 denier material clearly has a bilinear elastic modulus. The applied coating will to varying degrees inhibit the movement of the yarns. It can be seen, in Table 1, that the fraction of coated fabric thickness taken by the coating is greater for the 200 denier material. In addition, the areal density of the coating is less for the 840 denier material. From the responses shown in Figure 5 and data in Table 1, it was reasoned that the effect of the coating on the yarn rotation for the 840 denier material can be neglected for the purposes of this study.

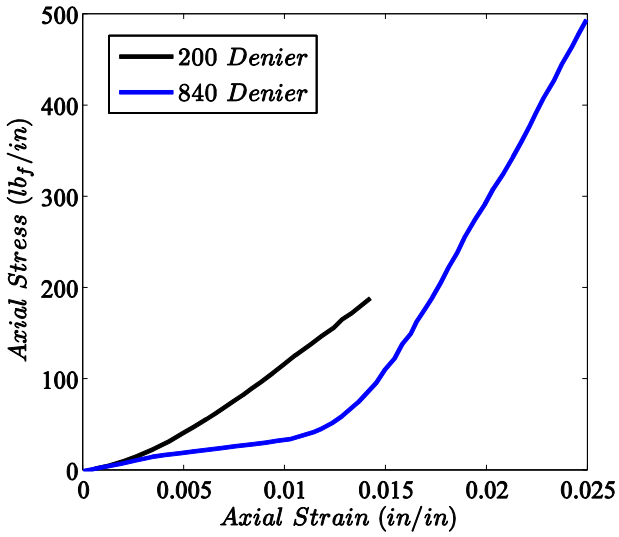

Figure 5: Axial Stress vs. Axial Strain

Table 1. Fabric Properties.

Denier (w x f)	Thread Count (yards/in)	Uncoated Fabric Thickness (in)	Coated Fabric Thickness (in)	Uncoated Areal Density (oz/yd^2)	Coated Areal Density (oz/yd^2)	Coating Add-On (oz/yd^2)
200	40 x 40	0.005	0.008	2.1	8.0	5.9
840	26 x 26	0.010	0.014	5.8	10.2	4.4

Now that the fabric material data was in place for later validation, attention was turned to the yarn data. A discussion on the elastic properties of the yarn, as well as, the fabric architecture will be presented after some fundamental information about the material model is provided.

B. Material Model

The following section provides a brief overview of the material model developed by Tabiei and Ivanov. The model uses a meso-mechanical approach in that it models the yarn interactions. The foundation of the model is the Representative Volume Cell (RVC) shown in Figure 6 on the left. The RVC, at the meso level, is constructed to represent the periodic structure of the fabric. While most other meso scale models use cell with its sides parallel to fiber directions, this model aligns its diagonals with the fiber directions. A zoomed in view of the RVC is shown in Figure 6 on the right. It is divided into 4 sub cells to take advantage of symmetry.

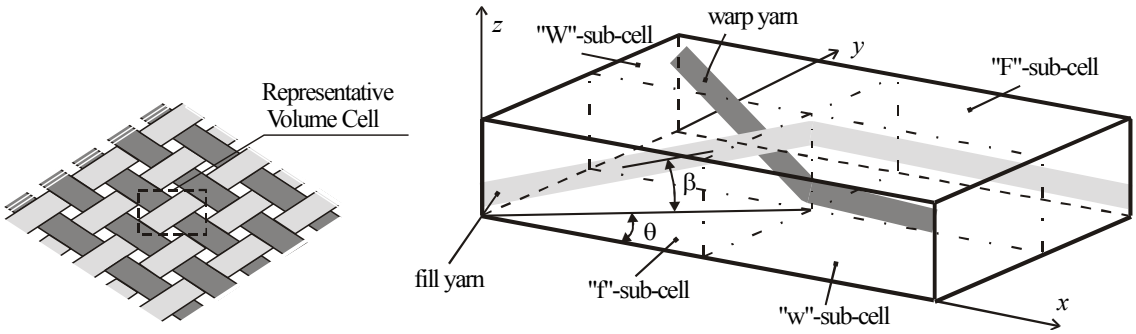

Figure 6: RVC (Left)[20], Sub-Cells (Right)[20]

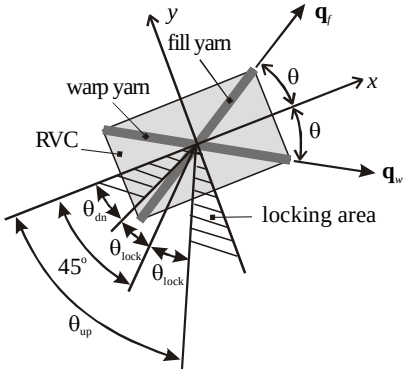

Figure 7: Yarn Locking Schematic[20]

There are two angles shown in the figure above. These define the orientation of the yarns and will change as a result of deformation. The braid angle, θ, is assumed to be the same for both the warp and the fill yarns. This is not always true in reality, but rather is an approximation. The undulation angle, β, is defined independently for the warp and fill yarns. Do to the assumptions with this models geometry, the undulation angle is the only means for differentiating between the warp and fill yarns.

As discussed earlier, the yarns will rotate in a similar manner to that of a trellis mechanism until some locking angle is reached and the yarns begin to behave as an elastic continuum. This locking angle is an input to the model and is seen, in the context of the RVC, in Figure 7. The implementation of the pre and post locking phases is implemented through the yarn stiffness matrix; which is provided in Equation 1. It is assumed that the yarn is modeled as an anisotropic continuum. The subscripts in Equation 1 represent material coordinate system components of the yarns; with the "1" direction running axial with the length of the yarn and "2" and "3" fulfilling the requirements for an orthogonal basis. A transformation matrix is used to rotate vectors in material coordinate system to the RVC coordinate system shown in Figure 6. The shear moduli are augmented by the discount factor, μ. Before locking, μ is a small number so that the yarns have low stiffness or low resistance to shear deformation. This allows the large rotations of the yarns. This term can be thought of as the amount friction between the yarns. After locking, μ is equal to 1 and the yarns regain their shear stiffness. A

tolerance, $\Delta\theta$, is defined to eliminate instantaneous changes in μ as θ approaches θ_{lock}. The discount factor is a function of θ, which in turn is a function of the unit direction vectors, q_f and q_w, that define the yarns orientation. The method by which the unit direction vectors are updated at each time step is now discussed.

$$\underline{\underline{C}} = \begin{bmatrix} \frac{1}{E_1} & -\frac{\nu_{12}}{E_1} & -\frac{\nu_{12}}{E_1} & 0 & 0 & 0 \\ -\frac{\nu_{12}}{E_1} & \frac{1}{E_2} & -\frac{\nu_{23}}{E_2} & 0 & 0 & 0 \\ -\frac{\nu_{12}}{E_1} & -\frac{\nu_{23}}{E_2} & \frac{1}{E_2} & 0 & 0 & 0 \\ 0 & 0 & 0 & \frac{1}{\mu G_{12}} & 0 & 0 \\ 0 & 0 & 0 & 0 & \frac{1}{\mu G_{23}} & 0 \\ 0 & 0 & 0 & 0 & 0 & \frac{1}{\mu G_{12}} \end{bmatrix}^{-1} \tag{1}$$

To understand how the yarn unit direction vectors are rotated as the element is deformed, the derivation of the deformation gradient in Tabiei's model is stepped through in more detail. First, it is beneficial to provide a physical understanding to the deformation gradient prior to defining it mathematically. The deformation gradient is a tensor that quantifies the shape change and material rotation. This property makes it better than strain as a more comprehensive measure of deformation in material elements. Consider the simple example provided in Figure 8. Let the shape on the left represent an undeformed material element and on the right, the deformed shape. By introducing horizontal and vertical axes, the undeformed element can be said to have unit length in both axes. It can be seen that the deformed element is stretched in both principal directions.

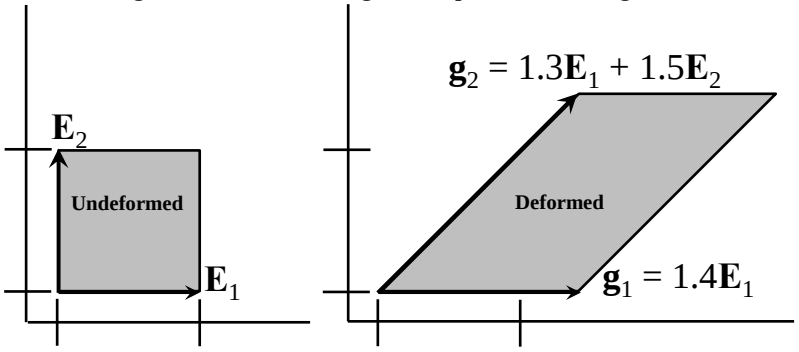

Figure 8: Determination of Deformation Gradient Graphically

The resulting direction vectors are expressed in terms of the initial unit direction vectors. Reading from the plot on the right, the components of the direction vectors can expressed in vector form as in Equation 2.

$$\underline{g_1} = \{1.4 \quad 0\}^T \quad \textit{and} \quad \underline{g_2} = \{1.3 \quad 1.5\}^T \tag{2}$$

Assembling these components into a 2 x 2 matrix results in a 2D deformation gradient tensor for this element.

$$\underline{\underline{F}} = \begin{bmatrix} 1.4 & 1.3 \\ 0 & 1.5 \end{bmatrix} \tag{3}$$

Working from the derivation in Crisfield[21], consider an element d**X** that has original coordinates **X**. Let the element be moved to new coordinates **x** resulting from displacement **u** as shown in Figure 9. This can be written in vector form and differentiated to give the later part of Equation 4.

$$\underline{x} = \underline{X} + \underline{u} \qquad \Rightarrow \qquad \underline{dx} = \frac{\partial \underline{x}}{\partial \underline{X}}\underline{dX} = \underline{\underline{F}}\,\underline{dX} = \frac{\partial\left(\underline{X} + \underline{u}\right)}{\partial \underline{X}}\underline{dX} \tag{4}$$

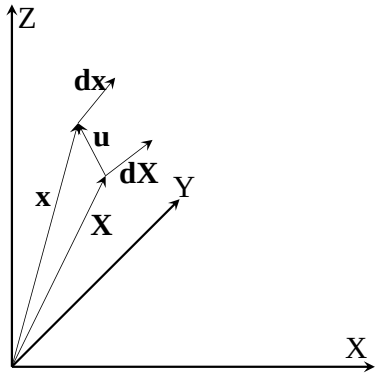

Figure 9: Position Vectors

Expanding upon this, Equation 5 introduces the mathematical representation of the deformation gradient (**F**) which can be expressed, as is shown in the middle matrix below, as the identity matrix plus the displacement derivative matrix. In the case of infinitesimal strains, the deformation gradient can be expressed in the final form of Equation 5. This form works well with the explicit finite element method because of the inherently small time steps used in this method.

As stated earlier, the directions of both the warp and fill yarns are determined buy the unit direction vectors, q_w and q_f, respectfully. At the beginning of the simulation, the unit direction vectors are defined based on Equation 6. After computing the deformation gradient matrix, using the strains at each time step, the updated direction vectors of each yarn are computed and normalized, as in Equation 7, to remain unit vectors.

$$\underline{\underline{F}} = \begin{bmatrix} \frac{\partial x}{\partial X} & \frac{\partial x}{\partial Y} & \frac{\partial x}{\partial Z} \\ \frac{\partial y}{\partial X} & \frac{\partial y}{\partial Y} & \frac{\partial y}{\partial Z} \\ \frac{\partial z}{\partial X} & \frac{\partial z}{\partial Y} & \frac{\partial z}{\partial Z} \end{bmatrix} = \begin{bmatrix} 1+\frac{\partial u}{\partial X} & \frac{\partial u}{\partial Y} & \frac{\partial u}{\partial Z} \\ \frac{\partial v}{\partial X} & 1+\frac{\partial v}{\partial Y} & \frac{\partial v}{\partial Z} \\ \frac{\partial w}{\partial X} & \frac{\partial w}{\partial Y} & 1+\frac{\partial w}{\partial Z} \end{bmatrix} = \begin{bmatrix} 1+\Delta\varepsilon_1 & \frac{\Delta\varepsilon_4}{2} & \frac{\Delta\varepsilon_6}{2} \\ \frac{\Delta\varepsilon_4}{2} & 1+\Delta\varepsilon_2 & \frac{\Delta\varepsilon_5}{2} \\ \frac{\Delta\varepsilon_6}{2} & \frac{\Delta\varepsilon_5}{2} & 1+\Delta\varepsilon_3 \end{bmatrix} \tag{5}$$

$$\underline{q_i} = \left\{ \cos\beta_i \cos\theta \quad \cos\beta_i \sin\theta \quad \sin\beta_i \right\}^{\mathrm{T}} \qquad for \quad i = f, w \tag{6}$$

$$\underline{q_i'} = \underline{\underline{F}}\,\underline{q_i} \quad \Rightarrow \quad \underline{q_i} = \underline{q_i'} \big/ \left\| \underline{q'} \right\| \qquad for \quad i = f, w \tag{7}$$

New values defining the orientation of the yarns are then calculated, as is shown in Equations 8 and 9, from the components of the unit direction vectors.

$$\beta_i = \sin^{-1}\left(q_{i3}\right) \qquad for \quad i = f, w \tag{8}$$

$$\theta = \frac{\tan^{-1}\left(q_{f2}/q_{f1}\right) - \tan^{-1}\left(q_{w2}/q_{w1}\right)}{2} \tag{9}$$

A homogenization method is used to obtain the effective elastic and shear moduli of the fabric based on the properties of the yarns. The details of this procedure are deferred and the reader is referred to the paper by Tabiei and Ivanov for a more detailed presentation of the model development. Numerical simulation results are now offered and compared to the experimental data described earlier in this paper.

IV. Numerical Examples

The experimental data used to validate this material model was obtained from a series of tests, by ILC Dover, to measure and characterize the normal and shear stress-strain behavior of textile fabrics relevant to IADs. To that end, four different test methods were used in that program: 1 for normal stress-strain and 3 for shear stress-strain. The uniaxial test method, used in the ILC testing, allows for the normal stress strain relationship of a sample to be obtained. Trellis Frame, Bias Extension, and Cylinder Biaxial testing were carried out for purposes of shear stress-strain characterization. While only one test for shear properties was necessary, all three were done for comparison

purposes. Simulations of these tests were replicated within LS-DYNA® and the results were compared to the experimental data.

Bias Extension Testing

The Bias Extension test is well suited for this material model. In preparation for actual testing, a simple rectangular sample is cut so that the yarn orientation is +/- 45° from an axis aligned with the loading direction. Due to the orientation of the RVC, a standard rectangular mesh aligns the yarns in this manner. Thus, the Bias Extension testing is perhaps a natural starting point for numerical simulations.

As described earlier in this paper, a fabrics shear behavior consist of several phases, such as deformation when the shearing forces at yarn intersections is too small to overcome friction, slippage of the yarns once that friction is overcome, and elastic deformation after yarn locking. While the shear modulus, G, is usually much less than the elastic modulus, E, in the warp and fill directions, it has a significant effect on the effective moduli on orientations not align with the warp and fill directions. The Bias Extension test method can be combined with uniaxial stress tests in the warp and fill directions to calculate shear modulus Equation 10[22].

$$G_{12} = \frac{1}{\frac{4}{E_{45}} - \frac{1}{E_1} - \frac{1}{E_2} + \left(\frac{\nu_{21}}{E_1} + \frac{\nu_{12}}{E_2}\right)} \tag{10}$$

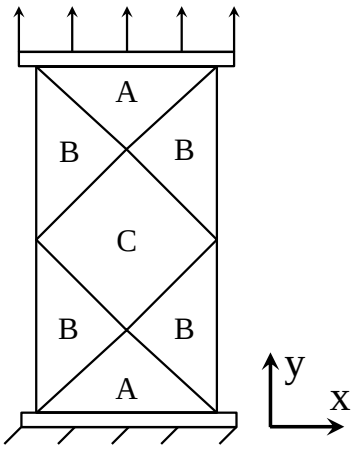

Figure 10: Bias Extension Deformation Zones

While the previous equation is a linear approximation, a nonlinear solution can be obtained using theory from large deformation continuum mechanics. Using the deformation gradient for two line elements, one originally aligned with the warp yarns and the other with the fill yarns, the Green-Lagrange strain tensor can be derived. In practice, line markings are made on the sample and tracked over time using photogrammetry. For each photo, the length of each line element is used to determine the stretch and orientation.

As load is applied to the sample, three distinct zones occur that contain different deformation modes as shown in Figure 10[22]. At the top and bottom in zone A, near the grips, little to no deformation occurs. In zone B, which surrounds the center region, is a transition zone where a mixture of shearing and extension occurs. Zone C, contains mainly shear deformation. This is the zone from which the measurements are taken.

1. Model Setup

The sample size used for the Bias Extension simulation is consistent with the dimensions used during testing. The height is 8.6 inches and the width is 3.5 inches. One of the assumptions made early on, was that the coating did not significantly the stiffness of the material. Thus, the uncoated fabric thickness of 0.010 inches was applied to the section of the model. The data reported for the Bias Extension test was load and crosshead extension rather than shear stress and strain. The cross head is converted to shear strain by taking advantage of the pure shear that occurs in the sample shown in Figure 10. The shear angle, θ, is defined in Equation 11.

$$\theta = \frac{\pi}{2} - 2\phi = \frac{\pi}{2} - 2\cos^{-1}\left[\cos\phi_0 + \frac{\delta}{2(H-W)\cos\phi_0}\right] \tag{11}$$

In the above equation, H = sample height, W = sample width, δ = displacement, and ϕ_0 is the initial half angle that the top corner Zone C makes with the vertical. ϕ_0 is assumed to equal 45° for this example.

Table 2. Model Inputs

Parameter	Value
ρ	1.44 g/cm^3
E_1	99.1 GPa
E_2	7.4 GPa
G_{12}	2.5 GPa
G_{23}	5.0 GPa
ν_{12}	0.2
ν_{23}	0.2
β_f	1°
β_w	1°
θ_{lock}	5°
$\Delta\theta$	0.5°
μ_0	1e-5

The sample of Kevlar 129 was simulated with the elastic material properties and fabric architecture shown in Table 2. These values are taken as estimates from Tabiei and Ivanov. The model was composed of 3705 reduced integration, 4-node membrane elements. At the base of the model, all degrees of freedom are fixed to apply a clamped boundary condition. The top nodes allow for displacement in the vertical direction. An axial load was applied to the sample by prescribing a 0.25 inch displacement at the top nodes. This displacement is derived from Equation 11 and attempting to match the maximum shears strains in the experimental data. The displacement was applied incrementally in a linear manner over the length of the simulation. The resulting load was calculated by summing all the nodal reaction forces in the vertical direction at the top nodes. Locally orthotropic material axes can be defined within this material model by rotating the material axes about the element normal. This option was not necessary for the Bias Extension test, as the RVC already aligns the yarns in the desired orientation. This option will be discussed for the uni-axial simulation.

2. Results

The following section presents the results of the bias extension simulations. The nominal model inputs provided in Table 2 are suggested values and should be varied from the nominal to assess the sensitivity of the model. Two of the input parameters, μ and θ_{lock}, were observed to effect the simulation results to a large degree. These parameters were varied from the nominal values and plotted along with the experimental data.

The discount factor, μ, scales down the shear moduli of the yarn before the yarns lock. An initial value for this parameter should be set to provide negligible shear resistance and tension in the yarns when loaded in the bias direction and before locking. On the right, Figure 11 shows three values of the discount factor plotted against an experimental data sample (Item B). Figure 11 also shows contour plots of the Green-Lagrange strain in the vertical direction. The contours show the same behavior shown earlier in Figure 10. The central zone appears to elongate as the initial discount factor is increased. This is caused by the shear moduli providing a higher resistance to rotation and thus the distinction between the transition zones and the shear dominated zone is blurred. The suggested value does not fit well with the experimental data, suggesting that there is more friction between the yarns for which the lowest value of the discount factor accounts. Increasing the discount factor by 1 and 2 orders of magnitude brings the simulation results closer to the experimental data. This simulation provides a means for selecting an appropriate value for the discount factor by choosing multiple values until the best fit of the force-strain curve is obtained. It is observed, however, that the simulation results are more non-linear than the experimental data. A better fit could possibly be arrived at by varying other input parameters, such as the $\Delta\theta$, to provide a wide transition from the free to the locked state.

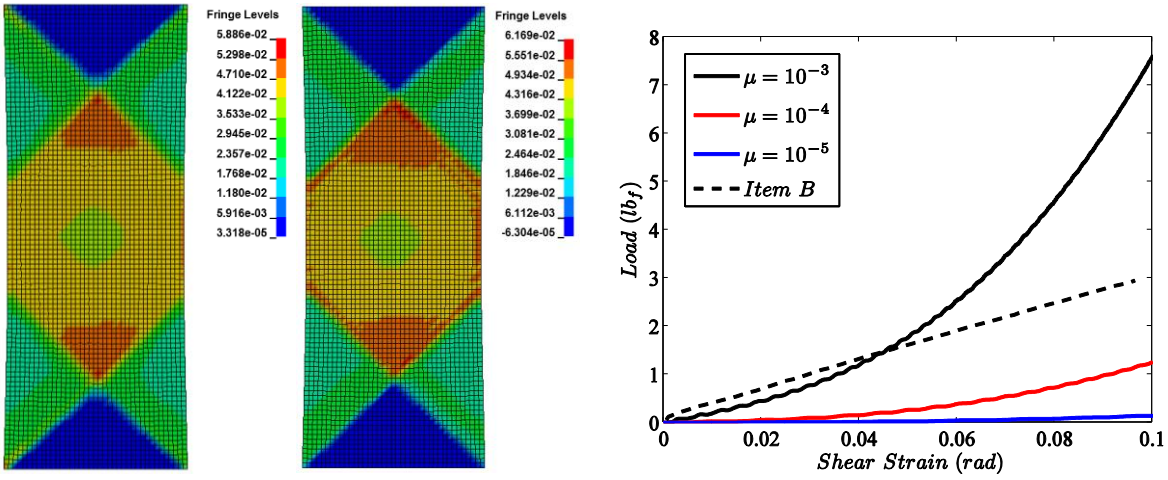

Figure 11: μ = 1e-3 (left), μ = 1e-5 (middle), Load vs. Engineering Shear Strain (right)

The locking angle was also varied from the nominal. Once the locking angle is reached, the shear stiffness is no longer scaled down and the samples stiffness increases. On the right, Figure 12 shows two values of the locking angle plotted. The experimental data is not plotted because the nominal value of the discount factor was utilized and thus, the experimental data would not fit on the plot. Figure 12 also shows contour plots of the Green-Lagrange strain in the vertical direction. The contours show the same behavior shown earlier in Figure 10. The contours represent the strain distribution at the final time step of the simulation. It can be seen that the zones are much more clearly defined for lower locking angle case. This is consistent with the expected continuum behavior of the material model after locking occurs. The plot on the right shows the materials shear stiffness increasing drastically toward the later end of the simulation. Similar to the discount factor, the bias extension simulation could serve as a method of tuning the parameters to fit the experimental data.

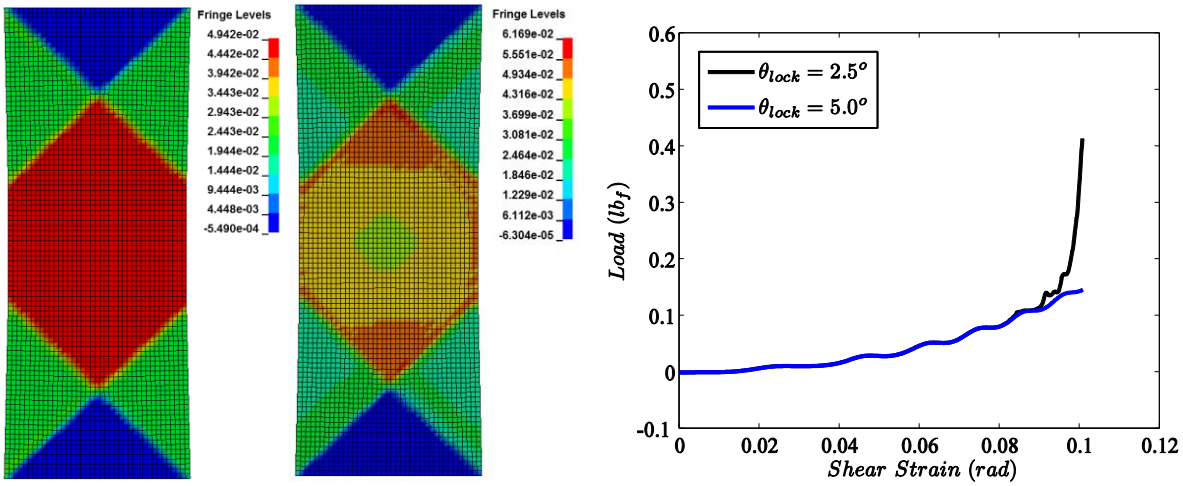

Figure 12: θ_{lock} = 2.5° (left), θ_{lock} = 5.0° (middle), Load vs. Engineering Shear Strain (right)

C. Uni-Axial

The uni-axial test is one of the simplest test methods for characterizing the normal stress-strain behavior of woven fabrics. In preparation for actual testing, a simple rectangular sample is cut so that the yarn orientation is 0/90° from an axis aligned with the loading direction. In contrast to the bias extension sample, the orientation of the RVC is not properly aligned for a standard rectangular. Thus, the uni-axial testing requires a rotation of the material axes for numerical simulations.

1. Model Setup

The sample size used for the uni-axial simulation is also consistent with the dimensions used during testing. The height is 6 inches and the width is 3 inches. Again, the uncoated fabric thickness of 0.010 inches was applied to the section of the model. The data reported for the uni-axial test was axial stress in units of lbf/in and axial strain in dimensionless units.

The same material was used for this simulation. The model was composed of 3705 reduced integration, 4-node membrane elements. At the base of the model, all degrees of freedom are fixed to apply a clamped boundary condition. The top nodes allow for displacement in the vertical direction. An axial load was applied to the sample by prescribing a 0.1575 inch displacement at the top nodes. This displacement is derived by attempting to match the maximum axial strains in the experimental data. The displacement was applied incrementally in a linear manner over the length of the simulation. A locally orthotropic material axis was defined by rotating the material axis about the element normal by an angle from a line in the plane of the element. It is defined by the cross product of a vector, **v**, with the element normal, **n** and is illustrated in Figure 13. This option was necessary for the uni-axial simulation because of the orientation of the RVC. The yarns are aligned with the diagonals of the RVC. The material axis must be rotated by the initial angle between the warp and fill yarns for the yarns to be aligned with the loading axis.

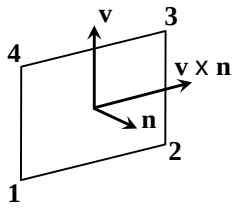

Figure 13: Locally Orthotropic Material Axis

Results

In defining the section properties of the material during model pre-processing, it is necessary to define a material thickness. It is common, however, to present stress data of fabrics in units of force per unit length. This is due to the large uncertainty the can come with measuring the fabric thickness. Thus, in the post processing of the results, the thickness was removed. The simulation data is plotted along with the experimental data in the warp and fill directions in Figure 14. A simulation time of 0.3 seconds was used, as it provides a relevant strain rate.

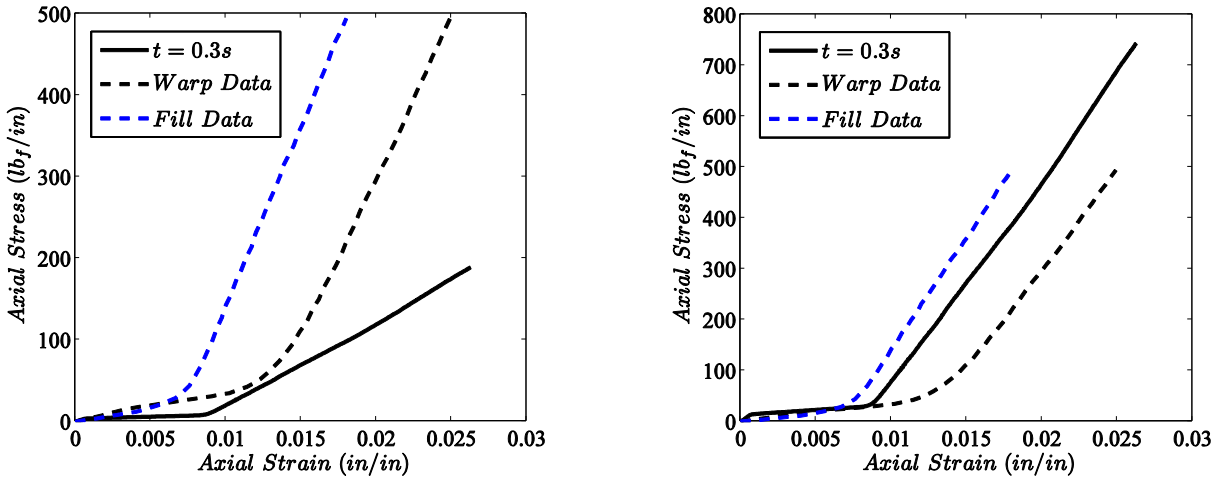

Figure 14: Axial Stress vs. Axial Strain for t = 0.01 inches (left) and for t = 0.0393 inches (right)

The first characteristic that is observed from the above results, is that the bilinear nature of the fabric. This indicates that the model is capable of capturing the low stiffness as the yarns rotate and the behavior after locking occurs. It was observed that the magnitude of the stress was not accurately represented. Because displacements are imposed at the top nodes, the resulting stress (force/unit area) is not a function of the material thickness. The nodal forces required to achieve this displacement will change with material thickness, however. Keeping that in mind, the material thickness was increased in the post processing to attempt to match the experimental data. Applying a thickness of 1mm (0.0393 in) resulted in the simulation data following the experimental data quite well. While in the reality the warp and fill yarns will behave differently under load, this material model, with the inputs chosen, cannot differentiate between them. Thus, it makes sense that the simulation data would fall in between the experimental data sets. It is unlikely that the adjusted material thickness of 4x the nominal thickness is a realistic number and rather serves as an additional tuning parameter to this model.

Using the same variables, the sensitivity of the material model in this loading condition was assessed. Figure 15 shows the results of that analysis. The results show a high sensitivity to these inputs. On the left, the discount factor is increased such that the shear modulus in is small but not negligible in the pre-locking phase. By increasing the initial value of the discount factor to 0.01 from 0.00001, the material never overcomes the simulated friction between the yarns and the trellising behavior is removed from the model. The locking angle is also very sensitive to variations from the nominal. The plot on the right of Figure 15, shows that material response follows the same stress-strain behavior until the locking angle is reached. Then the material transitions right into the region of higher stiffness. Comparing these results to the experimental warp and fill data, it is seen that both the discount factor and locking angle can be varied to align the simulated data with the experimental data. Furthermore, the locking angle can be used to distinguish between the warp and fill directions.

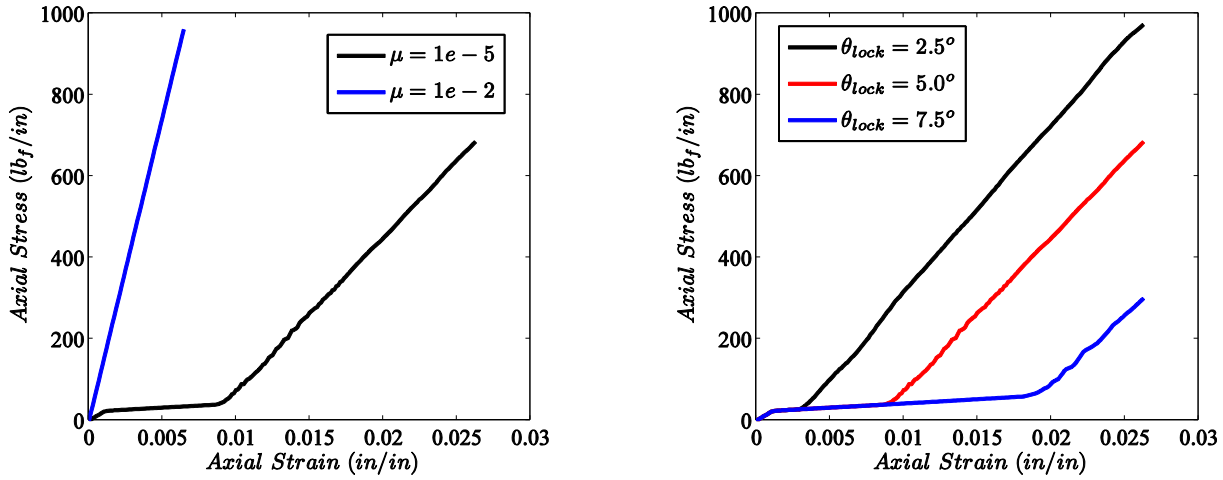

Figure 15: Axial Stress vs. Axial Strain for varying μ (left) and varying θ_{lock} (right)

Summary and Future Work

The explored mesomechanical material of a flexible woven fabric was shown to be capable of capturing the dual behavior corresponding to that of actual fabrics. Simulations replicating actual tests for the normal and shear properties of fabrics show the trellising behavior before yarn locking followed by the elastic behavior of the fabric after locking. The model shows the ability to obtain good agreement with experimental test data by varying the input parameters. In addition, the model was most sensitive to yarn locking angle and discount factor. While the model is capable of matching experimental data, the number of tuning parameters make the obtaining the necessary information to utilize this model prohibitive. The increased computational cost of this model, over the lower fidelity MAT_FABRIC material model is also an issue for large scale use. The source of experimental data for this study also includes data from trellis frame and cylinder biaxial testing. FE models similar to the ones shown in Figure 13 can be utilized to further explore this material model.

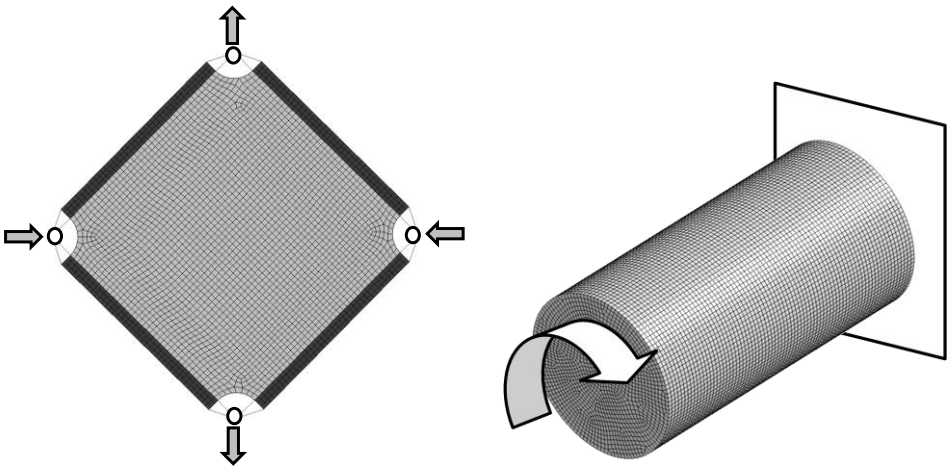

Figure 16: Trellis Frame (Left) and Cylinder Biaxial (Right) Meshes

Alternative methodologies can be explored that involves homogenizing the unit cell in a loosely couple manner. In order to make the material model explored in this paper more computationally efficient for larger models while still accounting for important fabric behavior, some detail is sacrificed. By modeling a small, but highly detailed, unit cell of fabric at the meso level and then applying a stand alone homogenization method to produce the material properties that can be applied to typical membrane element, the nonlinear and stress state dependent behavior of the

fabric can be captured without sacrificing computational cost in a macro level simulation. Following the diagram shown in Figure 17, a preliminary strategy could proceed as follows. After selecting a particular fabric, yarns can be extracted and subjected to experimental testing to obtain the constitutive properties. Next, the fabric architecture is replicated at the meso scale within a detailed unit cell model. Loads are applied to this model and the constitutive properties of the fabric are extracted from the numerical testing. The properties are then applied to a more computationally efficient material model. The homogenized element can then be applied to a large scale model. This methodology would require some knowledge of the expected state of stress over the large scale structure, but has the benefit of reducing the amount of experimental testing required to characterize the fabric at several states of stress and could eventually bring higher fidelity structural models for IADs forward in the design process.

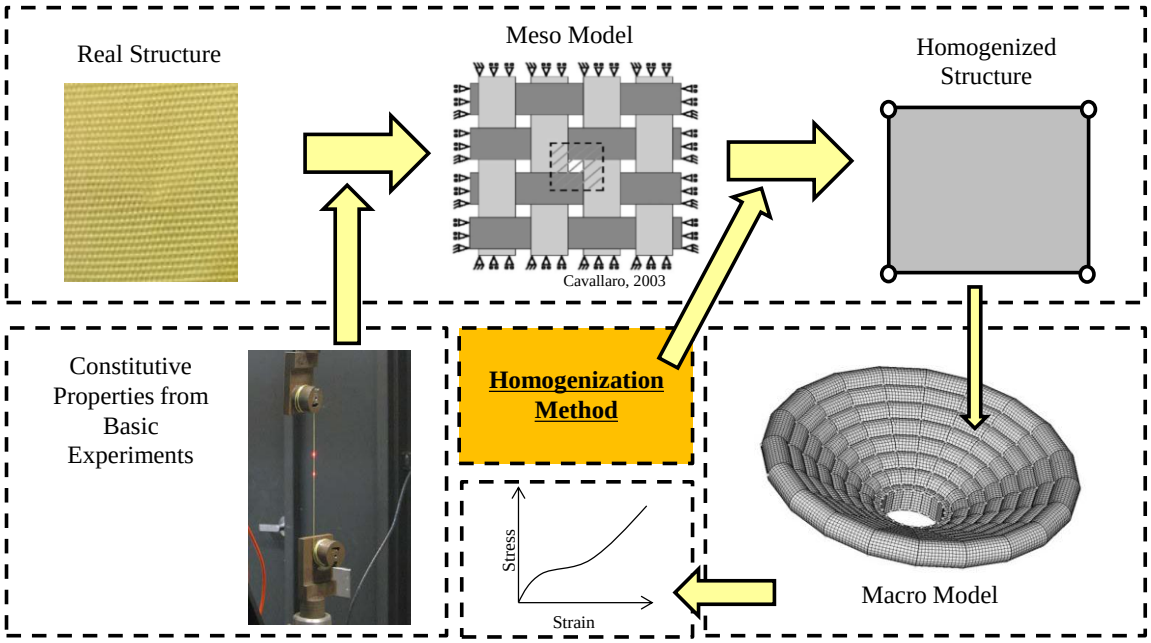

Figure 17: Alternative Meso-Scale Model Approach

Acknowledgments

The author would like to acknowledge Dr. Donald White of Georgia Tech for his help in framing this work, Dr. Ala Tabiei at University of Cincinnati for providing examples of his material models, Joe Welch of ILC-Dover for his assistance with LS-DYNA, and the Georgia Tech Space Systems Design Lab for their support and advice. This work was supported by a National Science Foundation Graduate Research Fellowship.

References

[1]Braun, R. D. and Manning, R. M., "Mars Exploration Entry, Descent, and Landing Challenges," Journal of Spacecraft and Rockets, vol. 44, no. 2, pp. 310-323, March-April 2007.

[2]Clark, I.G., Hutchings, A.L., Tanner, C.L., Braun, R.D., "Supersonic Inflatable Aerodynamic Decelerators for Use on Future Robotic Missions to Mars," *Journal of Spacecraft and Rockets*, Vol. 46, No. 2, 2009, pp. 340-352.

[3]Clark I.G., "Aerodynamic Design, Analysis, and Validation of a Supersonic Inflatable Decelerator," Ph.D. Dissertation, Daniel Guggenheim School of Aerospace Engineering, Georgia Institute of Technology, Atlanta, GA, 2009.

[4]Tanner, C.L., Cruz, J.R., Hughes, M.F., Clark, I.G., Braun, R.D., "Subsonic and Transonic Wind Tunnel Testing of Two Inflatable Aerodynamic Decelerators," *7th International Planetary Probe Workshop*, Barcelona, Spain, 2010.

[5]Lindell, M. C., Hughes, S. J., Dixon, M., Wiley, C. E., "Structural Analysis and Testing of the Inflatable Re-entry Vehicle Experiment (IRVE)", 47th AIAA/ASME/ASCE/AHS/ASC Structures, Structural Dynamics, and Materials Conference, AIAA-2006-1699, May 1-4, 2006.

[6]Smith, B. P., Tanner, C. L., Mahzari, M., Clark, I. G., Braun, R. D., and Cheatwood, F. M., "A Historical Review of Inflatable Aerodynamic Decelerator Technology Development," IEEEAC 1276, 2010 IEEE Aerospace Conference, Big Sky, MT, March 2010.

[7]Tanner, C. L., "Aeroelastic Analysis and Testing of Supersonic Inflatable Aerodynamic Decelerators," Ph.D. Dissertation, Daniel Guggenheim School of Aerospace Engineering, Georgia Institute of Technology, Atlanta, GA, 2012.

[8]Samareh, J. A., "Estimating Mass of Inflatable Aerodynamic Decelerators Using Dimensionless Parameters," *8th International Planetary Probe Workshop*, Portsmouth, Virginia, 2011.

[9]Kyser, A. C., "Deployment Mechanics for an Inflatable Tension-Cone Decelerator," NASA Contractor Report CR-929, November 1967

[10]Hutchings, A. L., Braun, R. D., Masuyama, K., and Welch, J. V., "Experimental Determination of Material Properties for Inflatable Aeroshell Structures," AIAA Paper 2009-2949, 2009.

[11]Bassett, R. J., Pastle, R., Pan, N., "Experimental Methods for Measuring Fabric Mechanical Properties: A Review and Analysis." Textile Research Journal. Vol 69. 1999. P. 866-875

[12]Lin, J. K., Shook, L. S., Ware, J. S., and Welch, J. V., "Flexible Material Systems Testing," NASA Contractor Report CR-2010-AC89D, May 2010.

[13]Murman, S. M., Suresh, S. S., "Modeling Effective Stiffness Properties of IAD Fabrics," AIAA 2011-2568

[14]Marrey, R. V., Sankar, B. V., "Micromechanical Models for Textile Structural Composites," NASA Contractor Report CR-198229, October 1995.

[15]Chen, X., "Modeling and Predicting Textile Behavior," Boca Raton, FL, Woodhead Publishing Limited, 2010.

[16]Kabche, J. P., Peterson, M. L., Davids, W. G., "Effect of Inflation Pressure on the Constitutive Response of Coated Woven Fabrics Used in Airbeams," Composites: Part B, Vol. 42, 2011, pp. 526-537

[17]Cavallaro, P. V., Johnson, M. E., Sadegh, A. M., "Mechanics of Plain-Woven Fabrics for Inflated Structures," Composite Structures, Vol. 61, 2003, pp. 375-393

[18]Komeili, M., Milani, A.S., "The Effect of Meso-Level Uncertainties on the Mechanical Response of Woven Fabric Composites Under Axial Loading," Computers and Structures, Vol. 90-91, 2012, pp. 163-171

[19]Peng, X. Q., Cao, J., "Numerical Determination of Mechanical Elastic Constants of Textile Constants," 15th Annual Technical Conference of the American Society for Composite, College Station TX, Sept. 25-27, 2000

[20]Tabiei, A., Ivanov I., "Computational Micro-Mechanical Model of Flexible Woven Fabric for Finite Element Impact Simulation," 7th International LS-DYNA Users Conference, 2001

[21]Crisfield, M. A., "Non-linear Finite Element Analysis of Solids and Structures," New York, NY, John Wiley & Sons, 1991.

[22]Williams, R. W., "Measuring and Modeling the Anisotropic Nonlinear and Hysteretic Behavior of Woven Fabrics," PhD diss., University of Iowa, 2010.